



Retinal vessel extraction by means of motion contrast, matched filter and combined corner-edge detector

Lei Yu ^{a,b,c,*}, Yue Qi ^{a,b,c}, Mingliang Xia ^b, Li Xuan ^a

^a State Key Laboratory of Applied Optics, Changchun Institute of Optics, Fine Mechanics and Physics, Chinese Academy of Sciences, Changchun 130033, Jilin, China

^b Medical Imaging Department, Suzhou Institute of Biomedical Engineering and Technology, Chinese Academy of Sciences, Suzhou, Jiangsu 215163, China

^c Graduate University of Chinese Academy of Sciences, Beijing 100049, China



ARTICLE INFO

Article history:

Received 4 September 2013

Received in revised form

10 December 2013

Accepted 18 December 2013

Available online 2 January 2014

Keywords:

Motion contrast

Matched filter

Combined corner/edge detector

Vessel segmentation

ABSTRACT

The microvasculature network of retina plays an important role in understanding of the retinal function and diagnosis of many diseases. Although it is possible to noninvasively acquire diffraction-limited resolution retinal images at microscopic cellular level, noises and other structures still make it difficult for diagnosis. In this paper, a new vessel extraction method is introduced. First, we use motion contrast method to trace the motion of the blood components and get the main vessel contour. Second, an improved matched filter method is applied to extract the vessel contour while the single-side edges are eliminated. Then, the combined corner/edge detector is adopted to eliminate the elongated fragments caused by the motion artifacts. Finally, we use mathematical morphology method to dilate the edges of vessels acquired in last step and obtain the exact contour of the vessels. The contrast of the vessels is significantly enhanced and the noises as well as other structures are effectively eliminated.

© 2014 Elsevier B.V. All rights reserved.

1. Introduction

The retina is a complex and multilayer structure, which can be noninvasively observed *in vivo*. The microscopic imaging of retina provides an important approach to early diagnosis of many sight-threatening retinal diseases, age-related macular degeneration as well as systemic diseases (diabetes, hypertension et al.) [1,2]. However, ocular aberrations limit the resolution of the retinal images. To overcome this obstacle, a variety of technologies were introduced into the retinal imaging systems (adaptive optics [3], optical coherence tomography [4], scanning laser ophthalmoscope [5], and so on). These technologies made it feasible to noninvasively acquire diffraction-limited resolution retinal images at microscopic cellular level.

Above all of the retinal structure, the microvasculature network plays a vital role in understanding of the retinal function and pathological changes because the microvasculature is the most predominant and stable structures appearing in the images. Since the huge quantity of images precludes strictly manual analysis while the noise and other structures out of focus will mislead the diagnosis, automated vessel extraction is necessary for retinal image processing and analysis [6].

The challenges of vessel extraction in retinal images can be summarized as follows:

- The widths of vessels are fickle, ranging from one pixel to more than 10 pixel.
- Some vessels are low contrast, especially for narrow vessels.
- Noises and other structures, which are out of focus, degenerate the images.
- The central reflex of the wider vessels makes it hard to be distinguished from a pair of side-by-side vessels.

The techniques on retinal vessel extraction may be roughly divided into categories based on: intensity edge methods [7,8], adaptive threshold methods [9,10], matched filter methods [11,12], mathematical morphology methods [13,14], region growing methods [15,16], Hessian-based methods [17,18] and machine learning methods [19,20]. All the methods concentrate on solving the challenges discussed above.

However, these methods discussed above mainly work on high-contrast retinal images (images obtained by fundus camera for example), which are high-contrast. They work badly on low-contrast retinal images (images obtained by AOSLO for example). This paper aims at the extraction of the capillaries, the width of which is less than 10 μm, in low-contrast retinal images (images obtained by AOSLO for example). As far as the authors know, there is no extraction method working on this kind of images. In this paper we introduce a new vessel extraction method, aiming at

* Corresponding author at: Chinese Academy of Sciences, Changchun Institute of Optics, Fine Mechanics and Physics State Key Laboratory of Applied Optics, Changchun 130033, Jilin, China. Tel.: +86 512 69588116; fax: +86 512 69588088.

E-mail address: yerlee@live.cn (L. Yu).

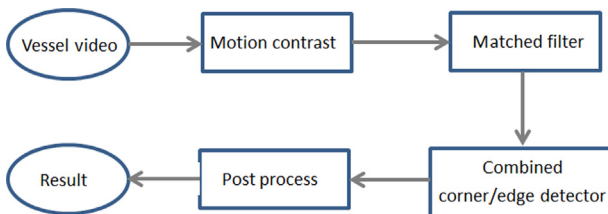


Fig. 1. Flow chart of vessel extraction algorithm by means of motion contrast, matched filter and combined corner/edge detector.

solving the first three challenges discussed above. Because the forth challenge can be overcome by so-called forward scatter method during imaging procedure [21]. The flow chart of the main algorithms is shown in Fig. 1.

The vessel video is acquired with an Adaptive Optics scanning laser ophthalmoscope (AOSLO). The video is 30 fps for 2 s monitoring the same region ($275 \mu\text{m} \times 286 \mu\text{m}$) of the retina. The imaging wavelength is 840 nm, at which waveband some components of blood reflect the light while other components of blood absorb the light. So we can see white flow parcels travelling through vessels. There is still debate in the field as to what the “white parcels” represent. According to Ref. [22], the motion of the parcels will adhere to the vessel walls. Then we can extract the vessel contour by tracing the motion of these white parcels. Because of the error of image registration and motion artifacts, there are many noises in the motion contrast image. Subsequently, we introduce a new multiple-scale matched filter method to distinguish vessels from false edges. To eliminate the effect of motion artifacts, we apply the combined corner/edge detector to the vessel image. Because the combined corner/edge detector has different responses to corners and edges, a local adaptive threshold is applied to acquire the edges which stand for the vessels. Finally, we smooth the vessels in the image through a series of post procedures.

This paper is organized as follows: In Section 2, we discuss the techniques and methods in detail. Then, the experimental condition and result are shown in Section 3. At last, we conclude this paper in Section 4.

2. Description of the methods

2.1. Motion contrast method

The blood mainly contains three components: plasma, erythrocytes and leukocytes. The light absorptions of these components are different at the imaging wavelength. So some components in the retinal image are white parcels while the other components of vessels are dark background, as shown in Fig. 2.

The white parcels travel through the vessels as marked in Fig. 2. Even if the vessels are dark background, the contrast is too low to distinguish the locations of vessels. This is because the photoreceptors are also white dots in the images. The photoreceptors have waveguide properties to return light directly back through the pupil [23]. So the light reflectance of photoreceptors is high as well. The centerline of the vessels is shown in Fig. 2(f).

The low contrast between vessels and background makes it impossible to extract the vessel contour using traditional methods. Since the white parcels travel along the vessel wall, we can make use of the motion of these white parcels to extract the vessel contour. The motion contrast method is similar to the one used in Ref. [24]. The motion contrast method is based on variance map between images, so the images must be cropped into the same size in pixels and the same region of retina. Then, these images pass through a median filter to eliminate the effect of noise. It is also

important that the images in the sequence have the same L^2 norm.

$$\|I\|_2 = \sqrt{I(x_1, y_1)^2 + I(x_2, y_2)^2 + \dots + I(x_n, y_n)^2} \quad (1)$$

here, I is the retinal image, $I(x_1, y_1), I(x_2, y_2), \dots, I(x_n, y_n)$ are the pixels of I . $\|\cdot\|_2$ denotes the L^2 norm.

Once the procedures discussed above have finished, we can go on to trace the motion of the white parcels along the vessels. A mean image $\bar{M}(x, y)$ is calculated from all of the images.

$$\bar{M}(x, y) = \frac{1}{N} \sum_{i=1}^N I_i(x, y) \quad (2)$$

where $I_i(x, y)$ represents the intensities of frame i in the video. N is the number of frames in the video. We use \bar{M} as reference image to construct division image $D_i(x, y)$

$$D_i(x, y) = I_i(x, y) / \bar{M}(x, y) \quad (3)$$

In the division image $D_i(x, y)$, pixels at the location of white parcels have large intensities while the pixels at the other parts have small intensities around 1. That is because the other parts of the image are stable when the white parcels are changeable. Then, a threshold, which is slightly larger than 1, is applied to the division images $D_i(x, y)$ to eliminate the stable background. Finally, all the division images $D_i(x, y)$ are synthesized into a single image (motion contrast image).

As shown in Fig. 3(b), the vessel contour is well detected, but we find that there are many white dots in the background, which degenerate the motion contrast image. From the size and distribution of the dots, we consider that it may be caused by two reasons:

- (1) The error of image registration: the images of the video are manually registered, and the main error of image registration is the shift from its original location. This kind of error will cause the motion contrast image degenerate on the whole scale of image.
- (2) The oscillations of the photoreceptors: the reflectance of some photoreceptors fluctuates within a second or two, which is in accordance with the time for imaging. In some cases, the photoreceptors disappeared and then reappeared [25]. This kind of error will lead to the local variance in some region. The intensity and location of the variance are random.

To eliminate these errors, a combined corner/edge detector is introduced and it will be discussed in Section 2.3.

2.2. Matched filter method

The matched filter method evaluates the correlation between image regions, which potentially contain a blood vessel segment, and the two-dimensional matched-filter masks, which approximate the typical blood vessel segments. If the manually selected blood vessel segments are available, the matched-filter masks can be constructed accordingly [26]. However, there is not any priori knowledge of the vessel images in our case. And our purpose is extracting the vessels automatically. So a reasonable matched-filter mask should be constructed. Since the distribution along the normal direction of the vessels is similar to one-dimensional Gaussian distribution, the matched-filter mask can be derived basing on Gaussian distribution [27].

The tangential distribution of traditional two-dimensional matched-filter mask is constant. That will exaggerate the contribution of the neighbor pixels and result in false vessels, as shown in Fig. 4.

We can see in the figure that: (1) The segments around the corner of vessels exceed the vessel contour and produce false

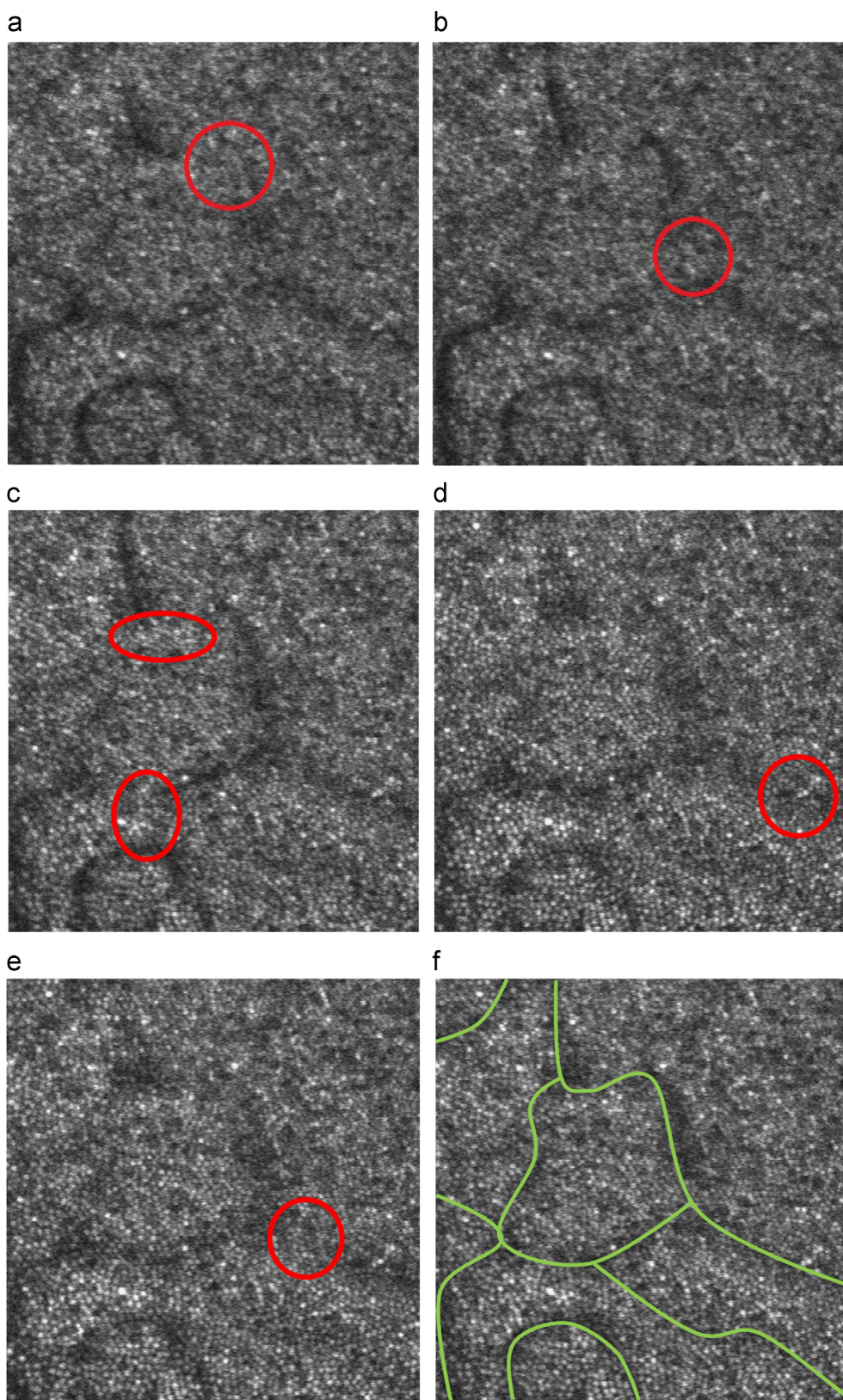


Fig. 2. High resolution retinal images acquired by AOSLO using an 840 nm laser. These images are from the video offered by Johnny Tam from the University of California, Berkeley. (a) Retinal image with white parcel (shown in red circle). (b) Retinal image with white parcel. (c) Retinal image with white parcel. (d) Retinal image with white parcel. (e) Retinal image with white parcel. (f) The manually labeled centerline of vessels. (For interpretation of the references to color in this figure legend, the reader is referred to the web version of this article.)

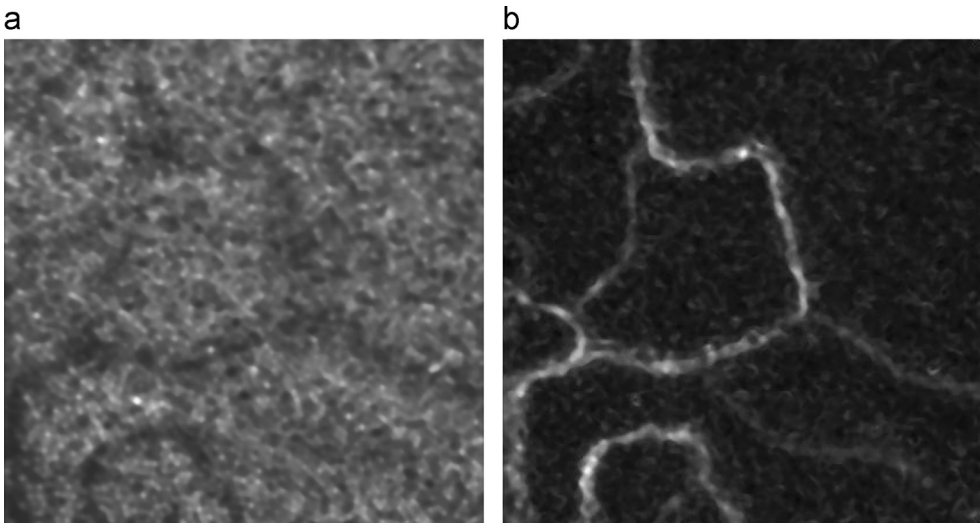


Fig. 3. (a) Reference image. (b) Motion contrast image.

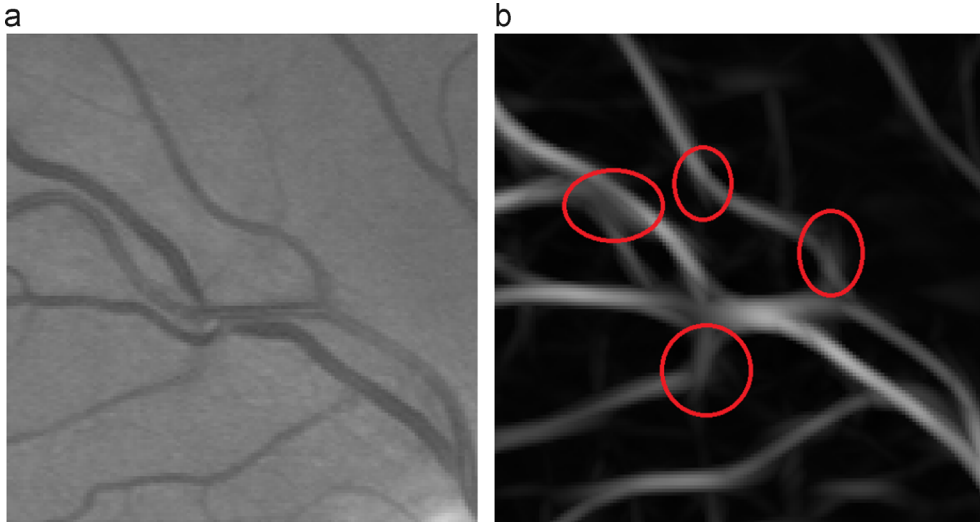


Fig. 4. (a) Vessel image with noise; (b) vessel segments with traditional mask.

vessels. (2) If two or more vessels are closed to each other, the segment between them will form a false conjunction.

To solve this problem, we introduce a new two-dimensional matched-filter mask. The distribution of the normal direction is a second-order derivative of Gaussian while the distribution of the tangential direction is Gaussian distribution.

$$g2nd(u, \sigma_u) = \frac{(u^2 - \sigma^2)}{\sigma^2} \times \exp\left(-\frac{u^2}{2\sigma^2}\right) \quad (4)$$

where $g2nd(u, \sigma_u)$ is the second-order derivative of Gaussian function with standard deviation σ_u . u represents one-dimensional pixel location.

$$g(v, \sigma_v) = \exp\left(-\frac{v^2}{2\sigma_v^2}\right) \quad (5)$$

where $g(v, \sigma_v)$ is Gaussian function with standard deviation σ_v , v represents one-dimensional pixel location. Then, the matched-filter response can be expressed as:

$$R(u, v; \sigma_u, \sigma_v) = \int_{-\infty}^{\infty} \int_{-\infty}^{\infty} g2nd(u - u'; \sigma_u) \times g(v - v'; \sigma_v) \times I(u', v') du' dv' \quad (6)$$

where $I(u', v')$ is the intensity of image at location (u', v') .

In order to extract vessels with a variety of widths, a group of multiple-scale matched-filtering masks (i.e. the value of σ_u is changeable, but the value of σ_v is constant) are applied to the vessel image. Then, the matched-filtering responses are combined to form the vessel contour. We choose the image in DRIVE databases to test the method proposed. The image, matched-filter mask, matched-filter response and manually labeled vessel are shown in Fig. 5.

From Fig. 5, we can see that this matched-filter method can detect all the manually labeled vessels. But there are many false vessels in the response image (Fig. 5(d)). These false vessels may be caused by the single edge in the original image (Fig. 5(a)). To eliminate the false vessels caused by single edge, another mask based on first-order derivative of Gaussian function is applied in this method.

To simplify the illustration, we consider that the vessels and single edges are the ideal step as shown in Fig. 6(a) and (b). The responses of vessels and single edges for both masks are shown in Fig. 7, respectively. We can find that the response of vessels for first-order derivative of Gaussian function (first-order mask) has a maximum at pixel $u - \sqrt{\sigma_u}$ and a minimum at pixel $u + \sqrt{\sigma_u}$ while the response of vessels for second-order derivative of Gaussian function (second-order mask) only have a maximum at pixel u . On the other hand, the response of single edges for first-order mask

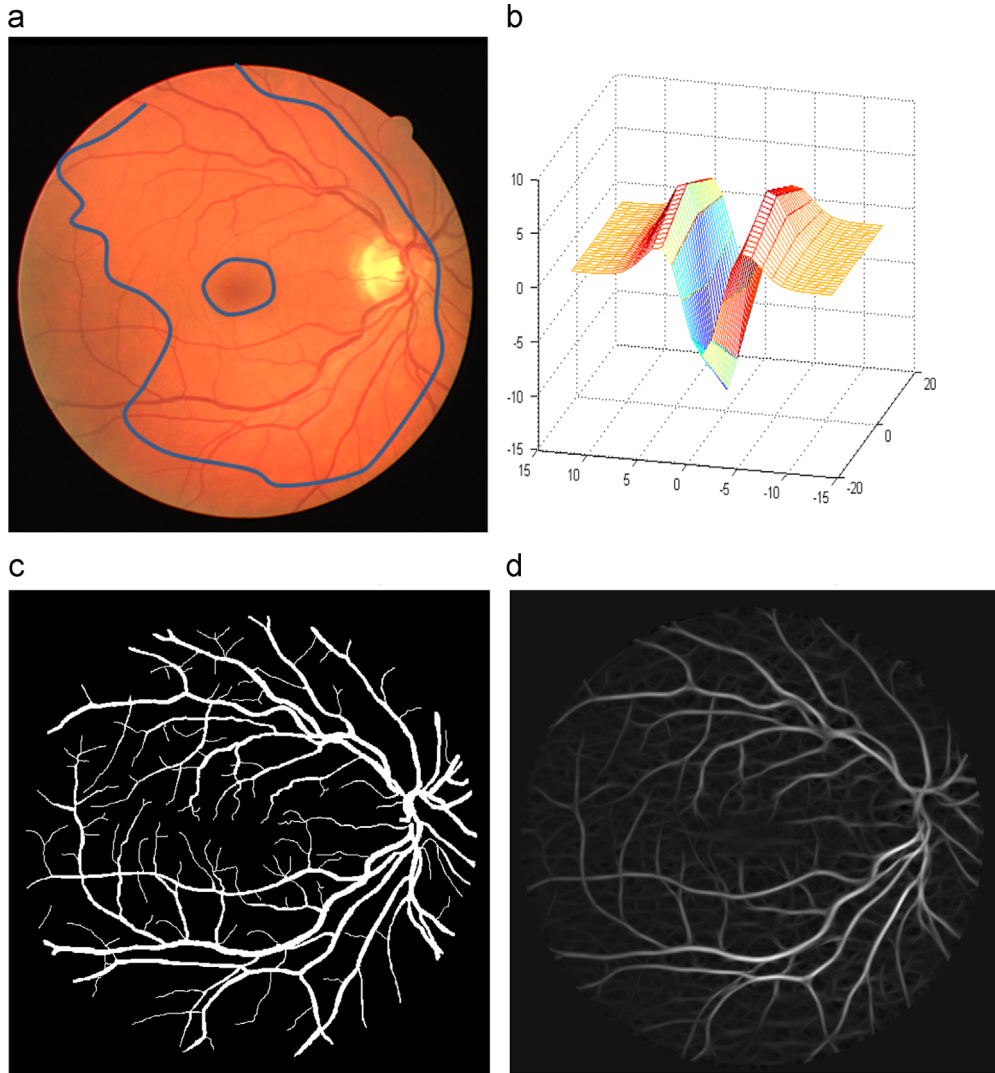


Fig. 5. The test result of matched-filter method with DRIVE databases. (a) The original vessel, (b) the matched-filtering mask, (c) the manually labeled vessels and (d) the matched-filter response.

only has a minimum at pixel u while the response of single edges for second-order mask has a maximum at pixel $u - \sqrt{\sigma_u}$ and a minimum at pixel $u + \sqrt{\sigma_u}$. We can use this difference to distinguish vessels from single edges. The responses of original image for both first-order mask and second-order mask are calculated, respectively. For every local maximum pixel u in the response for second-order mask, if there is a maximum at pixel $u - \sqrt{\sigma_u}$ in the response for first-order mask and a minimum at pixel $u + \sqrt{\sigma_u}$ in the response for first-order mask, then the pixel u belongs to vessels. Otherwise, this pixel u belongs to single edge and should be eliminated from the response for second-order mask. Once every local maximum pixel is judged by the method discussed above, the effect of single edges is eliminated as shown in Fig. 8.

From Fig. 8(b), we can see that most of the vessels are extracted while the effect of single edges is eliminated.

2.3. Combined corner/edge detector

As discussed in Section 2.1, the error of registration and the oscillations of photoreceptors will cause white dots in the background and degenerate the vessel extraction image. To solve this problem, we introduce a combined corner/edge detector [28]. The main purpose of this method is to detect corners and edges

respectively with different responses. To illustrate, we now consider a window patch (5 pixel \times 5 pixel for example) of the image:

- (1) If this window patch locates in a flat region (i.e. the intensities are almost constant in this region), then no matter which direction does the window patch move towards, the sum of the intensities in the window patch will have a small change (i.e. result in a small response).
- (2) If this window patch straddles an edge of vessel, then the sum of intensities in the window patch will have a small change (small response) when the window patch moves along the edge. However, the sum of intensities in the window patch will have a large change (large response) when the window patch moves perpendicularly to the edge.
- (3) If this window patch locates at a corner or a parcel of dots, then no matter which direction does the window patch move towards, the sum of the intensities in the window patch will have a large change (large response).

The schematic diagram is shown in Fig. 9.

According to the discussion above, we define the change of the sum intensities in the window patch as follows:

$$C(x, y) = \sum_{u,v} \{w(u, v) \times [I(x+u, y+v) - I(x, y)]^2\} \quad (7)$$

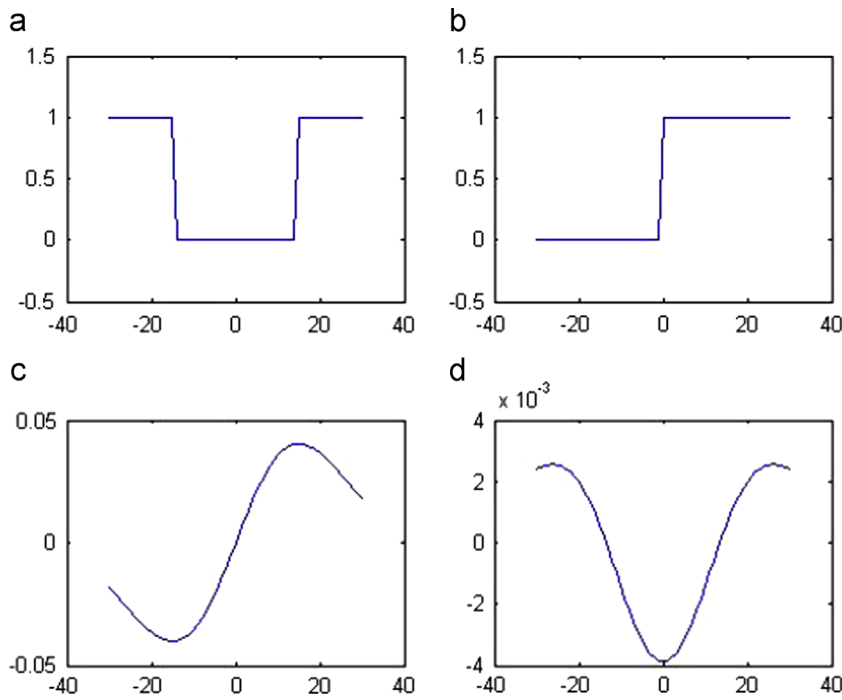


Fig. 6. Ideal vessel, single edge and mask. (a) Ideal vessel, (b) ideal edge, (c) first derivation of gaussian and (d) second derivative of gaussian.

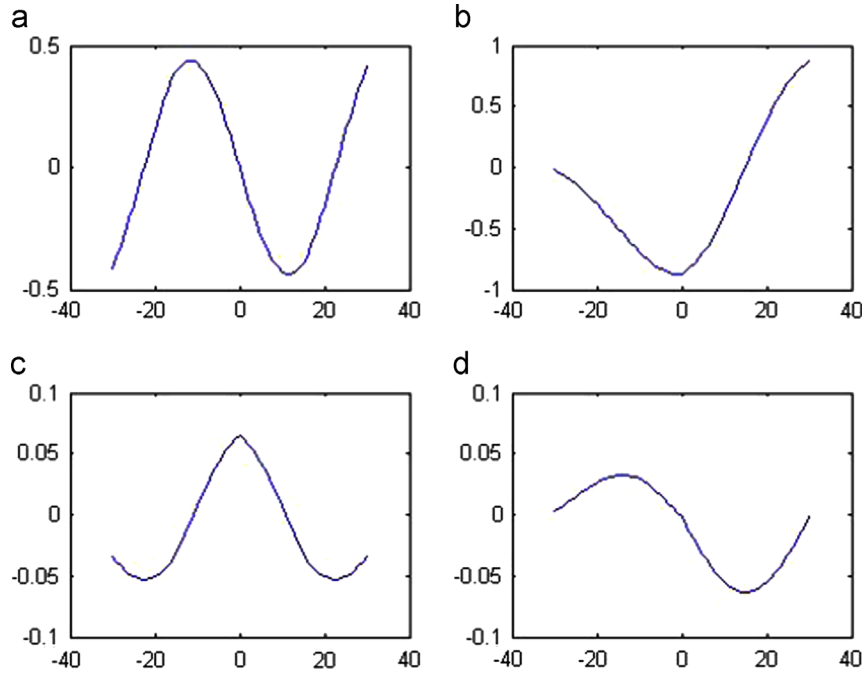


Fig. 7. The responses of the masks. (a) vessel response of gaussian 1st, (b) edge response of gaussian 1st, (c) vessel response of gaussian 2nd and (d) edge response of gaussian 2nd.

where $C(x, y)$ represents the change of the sum intensities in the window patch. (x, y) is the movement of the window patch w and (u, v) is the location of the pixel in the window patch. $I(u, v)$ is the intensity of the pixel located at (u, v) .

For a small movement (x, y) , the formula (7) can be approximated with the gradients as shown below

$$\begin{aligned} C(x, y) &\approx \sum_{u,v} w(u, v) \times \left[x \times \frac{\partial I}{\partial x} + y \times \frac{\partial I}{\partial y} \right]^2 \\ &= \sum_{u,v} w(u, v) \times \left[x^2 \times \left(\frac{\partial I}{\partial x} \right)^2 + 2xy \times \frac{\partial I}{\partial x} \cdot \frac{\partial I}{\partial y} + y^2 \times \left(\frac{\partial I}{\partial y} \right)^2 \right] \end{aligned} \quad (8)$$

$$\frac{\partial I}{\partial x} = I \otimes [-1, 0, 1], \quad \frac{\partial I}{\partial y} = I \otimes [-1, 0, 1]^T \quad (9)$$

where $(\partial I / \partial x)$ and $(\partial I / \partial y)$ are the gradients of the Image I for directions of x and y , respectively. Since x and y are scalars, the summation of formula (8) can be expressed by convolution

$$C(x, y) \approx x^2 \times \left(\frac{\partial I}{\partial x} \right)^2 \otimes w + 2xy \times \left(\frac{\partial I}{\partial x} \cdot \frac{\partial I}{\partial y} \right) \otimes w + y^2 \times \left(\frac{\partial I}{\partial y} \right)^2 \otimes w \quad (10)$$

where w is the window patch, and \otimes represents convolution. Then the response of the combined corner/edge detector can be defined

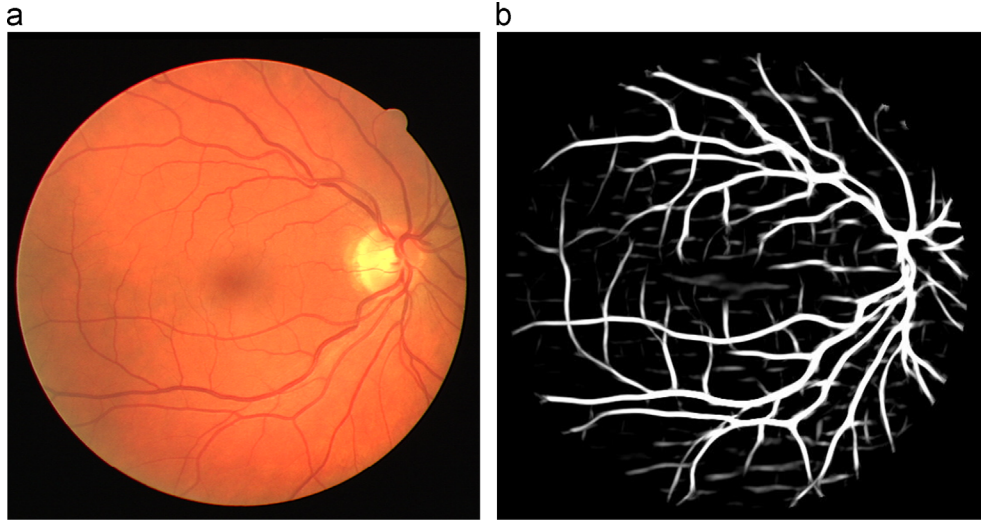


Fig. 8. (a) The original vessel image obtained by fundus camera; (b) the vessels extracted by the matched filter method.

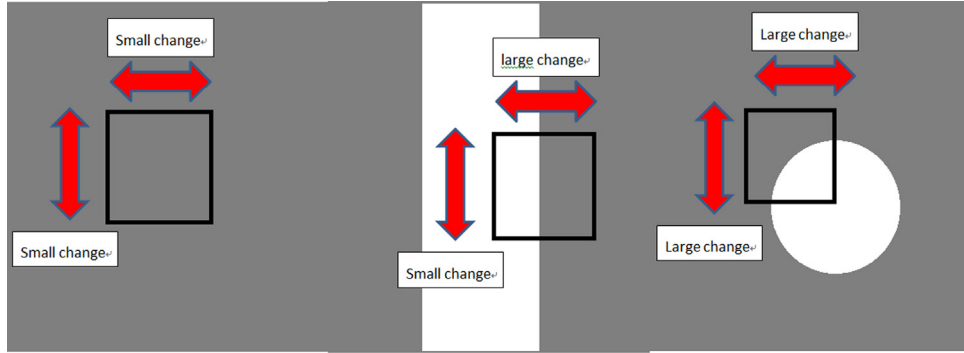


Fig. 9. The schematic diagram of the combined corner/edge detector.

as follows:

$$R(u', v') = \left(\frac{\partial I}{\partial x} \right)^2 \otimes w + \left(\frac{\partial I}{\partial y} \right)^2 \otimes w - k \times \left[\left(\frac{\partial I}{\partial x} \cdot \frac{\partial I}{\partial y} \right) \otimes w \right]^2 \quad (11)$$

where $R(u', v')$ is the response of the combined corner/edge detector at pixel (u', v') . (u', v') is the central pixel of the window patch w , k is a scalar, which should be determined by experiments.

If the window patch w locates at a flat region, for a small movement (x, y) (Note that, x and y are both positive.), $C(x, y)$ will be close to zero (i.e. $(\partial I/\partial x)^2 \otimes w, ((\partial I/\partial x) \cdot (\partial I/\partial y)) \otimes w$ and $(\partial I/\partial y)^2 \otimes w$ are all small.). So the response $R(u', v')$ is around zero.

If the window patch w straddles a vessel edge, for a small movement (x, y) along the edge of vessel, $C(x, y)$ will be close to zero. However, for a small movement (x, y) perpendicular the edge of vessel, $C(x, y)$ will be large enough. In other words, either $(\partial I/\partial x)^2 \otimes w$ is large while $(\partial I/\partial y)^2 \otimes w$ is small, or $(\partial I/\partial x)^2 \otimes w$ is small while $(\partial I/\partial y)^2 \otimes w$ is large. In this case, $((\partial I/\partial x) \cdot (\partial I/\partial y)) \otimes w$ is small. So $R(u', v')$ will have a large positive value.

If the window patch w is around photoreceptors, for a small movement (x, y) towards any direction, $C(x, y)$ will be large enough. That is to say, $(\partial I/\partial x)^2 \otimes w$, $((\partial I/\partial x) \cdot (\partial I/\partial y)) \otimes w$ and $(\partial I/\partial y)^2 \otimes w$ are all large. So $R(u', v')$ will have a negative value (we can adjust the value of k for a given image to achieve this).

Therefore, we can calculate the response $R(u', v')$ of the combined corner/edge detector for every pixel in the image. If the response $R(u', v')$ is a large positive value, the pixel (u', v') belongs to an edge of vessel. If the response $R(u', v')$ is close to zero, the pixel (u', v') belongs to a flat region. If the response $R(u', v')$ is

negative, the pixel (u', v') belongs to photoreceptors. By this means, we can distinguish vessels from photoreceptors.

3. Results

As mentioned above, the microvasculature network plays an important role in diagnosis of diseases. But the available high-resolution images cannot satisfy the requirement of diagnosis very well because the contrast of the vessels is not high enough as shown in Fig. 3(a). Our purpose is to use a combination of the methods discussed in Section 2 to enhance the contrast of the vessels. The image set, which is used for evaluating the proposed method in this paper, consists of 89 images obtained by AOSLO (The image set is offered by Johnny Tam from the University of California, Berkeley). First of all, motion contrast method is applied to the original video. The result is shown in Fig. 10(a).

From Fig. 10(a), we can find that the contrast of the vessels is enhanced by motion contrast method. The vessels are noticeable, however, there are also many white dots, which are caused by the error of image registration. Second, the multiple-scale matched-filter method with both first-order derivative of Gaussian and second-order derivative of Gaussian is introduced to extract the vessel contour and eliminate the single-side edges. The result is shown in Fig. 10(b). We can see that the main contour of vessels is kept while the single-side edges are eliminated. But there are also some noises in the result as labeled in the red circle. These noises are caused by the error of image registration and detected by the match-filter method as elongated fragments. To avoid the effect of

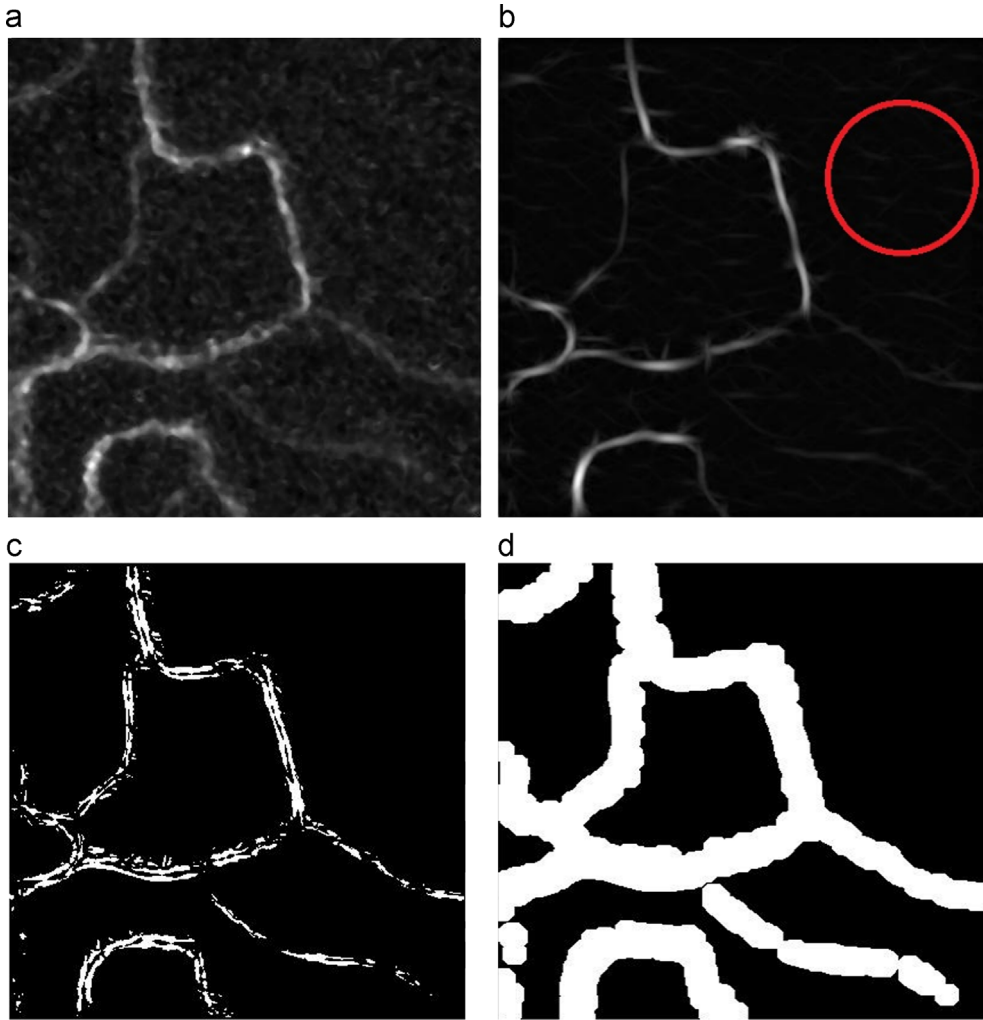


Fig. 10. The result of the methods proposed in Section 2. (a) motion contrast image, (b) matched filter response, (c) combined corner/edge detection and (d) mathematical morphology mask. (For interpretation of the references to color in this figure legend, the reader is referred to the web version of this article.)

the error of image registration, we apply a combined corner/edge detector to the motion contrast image (Fig. 10(a)). According to the features of the combined corner/edge detector discussed in Section 2.3, the vessels are detected as edges with large positive response while the photoreceptors are detected as corners with negative response. So we can use a threshold, which is slightly greater than zero, to extract the edges of vessels as shown in Fig. 10(c). Since the detector can only detect the edges of the vessels, we should adopt mathematical morphology method to restore the contour of vessels. A disk with the radius of 5 pixels is adopted to dilate the edges detected in Fig. 10(c). Then we get the dilated mask of the vessel contour as shown in Fig. 10(d). Finally, the dilated mask is used to implement so-called “and operation” with the match-filter image (Fig. 10(b)). That is we just reserve this part of matched filter image, which locates inside the dilated mask. The final result of the methods proposed in this paper is shown in Fig. 11(a). For the convenience of comparison, the original image is also shown in Fig. 11(b).

From Fig. 11 we can see that the contrast of the vessel is significantly enhanced by the methods proposed in this paper. Most of the vessel contour is extracted and satisfies the requirement for diagnosis. Although there is no ground truth segmentation of the vessels, the combined corner/edge detection can partly detect the boundary of the vessels. The yellow part in Fig. 11(a) is

detected as edges of vessels by combined corner/edge detection method and detected as vessels by the improved matched filter method. Therefore, this part of vessels definitely belongs to the real vessels. The red part, which is surrounded by the yellow part, also belongs to the real vessels. Because they are inside the edges, which are indicated by the yellow part, and have high matched filter response. The green part is detected as edges of vessels by combined corner/edge detection method, but the matched filter response of this part is low. Hence, this part possibly belongs to the real vessels to some extent. As for the red part, which is outside the yellow part, it has high matched filter response while it is detected as corner by the combined corner/edge detection. Hence, it may be some filaments attached to the vessels as shown in Fig. 11(a) (labeled by blue circles). By comparing this result with the motion contrast image, we think these filaments may be caused by the motion artifacts next to the vessels. These pixels are so closed to the vessels that they are detected as the white parcels floating in the vessels. Furthermore, these pixels are adhering to the vessels, so they cannot be detected by the combined corner/edge detector as corners. As a result, they are detected by the combined method as filaments. This is a drawback of the proposed methods and will be overcome by future work.

The time consumption for each step of the proposed method are listed in Table 1.

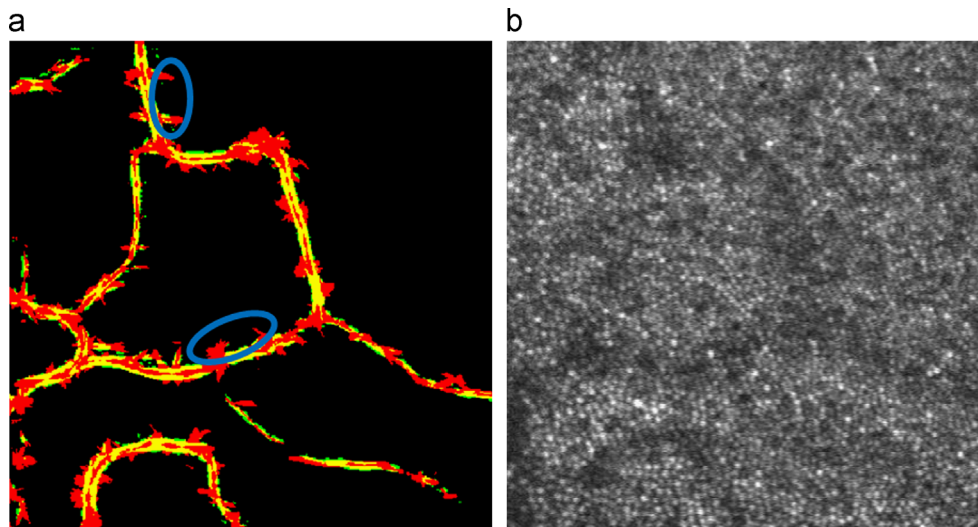


Fig. 11. (a) The final result of the proposed methods. (b) The original image. (For interpretation of the references to color in this figure legend, the reader is referred to the web version of this article.)

Table 1
Time consumption.

	MC	MF	CD	MM	Total
Time (s)	1.56	22.30	6.58	0.28	30.72

MC, MF, CD, MM stand for the step of Motion Contrast, Matched Filter, Combined corner/edge Detector and Mathematical Morphology, respectively. Total represents the total time consumption of the proposed methods. This experiment is conducted on the desktop computer with parameters as follows: CPU, Intel i3-2100 3.10 GHz; RAM, 4 G; OS, Windows7; Software, MATLAB R2009b.

4. Conclusion

Although it is possible to noninvasively acquire diffraction-limited resolution retinal images at microscopic cellular level, noises and other structures also make it difficult for diagnosis. In this paper, we propose a new vessel extraction method based on motion contrast, matched filter and combined corner/edge detector. First of all, motion contrast method is applied to trace the motion of blood components in the video (obtained by AOSLO). Since the white parcels travel along the vessel wall, we can make use of the motion of these white parcels to extract the vessel contour. There are also many noises in the motion contrast image at this time. Second, we use an improved matched-filter method to extract the main contour of the vessels. However, there are still some elongated fragments caused by the motion artifacts. Then, a combined corner/edge detector is adopted to distinguish the edge of vessels from the motion artifacts. Finally, we use mathematical morphology method to dilate the combined corner/edge detecting image and get the extracted vessels. From the result of this vessel extraction method, we can see that the contrast of the vessels is significantly improved and the noises as well as other structures are effectively eliminated.

Acknowledgements

This work has been supported by the National Natural Science Foundation of China (Grant nos. 60736042, 1174279 and 1174274). Thank Johnny Tam for offering the images used in this paper.

References

- [1] K.E. Talcott, K. Ratnam, S.M. Sundquist, et al., *Invest. Ophthalmol. Vis. Sci.* 52 (5) (2011) 2219.
- [2] Y. Kitaguchi, T. Fujikado, K. Bessho, et al., *Ophthalmology* 115 (10) (2008) 1771.
- [3] N. Kong, C. Li, M. Xia, et al., *J. Biomed. Opt.* 17 (2) (2012) 026001.
- [4] T. Torzicky, S. Marschall, M. Pircher, et al., *J. Biomed. Opt.* 18 (2) (2013) 026008.
- [5] S.H. Rasta, A. Manivannan, P.F. Sharp, *J. Biomed. Opt.* 17 (11) (2012) 116005.
- [6] W. Liu, T. Liu, W. Song, et al., *J. Biomed. Opt.* 18 (1) (2013) 016002.
- [7] A. Can, H. Shen, J.N. Turner, et al., *IEEE Trans. Inf. Technol. Biomed.* 3 (2) (1999) 125.
- [8] D. Koozekanani, K. Boyer, C. Roberts, *IEEE Trans. Med. Imaging* 20 (9) (2001) 900.
- [9] A. Hoover, V. Kouznetsova, M. Goldbaum, *IEEE Trans. Med. Imaging* 19 (3) (2000) 203.
- [10] X. Jiang, D. Mojon, *IEEE Trans. Pattern Anal. Mach. Intell.* 25 (1) (2003) 131.
- [11] F.P. Miles, A.L. Nutall, *IEEE Trans. Med. Imaging* 12 (2) (1993) 147.
- [12] S. Chaudhuri, S. Chatterjee, N. Katz, et al., *IEEE Trans. Med. Imaging* 8 (3) (1989) 263.
- [13] M.E. Martínez-Pérez, A.D. Hughes, A.V. Stanton, et al., Retinal blood vessel segmentation by means of scale-space analysis and region growing, in: Proceedings on Second International Conference on Medical Image Computing and Computer-assisted Intervention, Cambridge, England. 1679, 1999, pp. 90–97.
- [14] F. Zana, J.C. Klein, *IEEE Trans. Image Process* 10 (7) (2001) 1010.
- [15] M.A. Palomera-Pérez, M.E. Martínez-Pérez, H. Benítez-Pérez, et al., *IEEE Trans. Inf. Technol. Biomed.* 14 (2) (2010) 500.
- [16] M. Himaga, D. Usher, J.F. Boyce, et al., *Invest. Ophthalmol. Vis. Sci.* 42 (4) (2001) S702.
- [17] J. Staal, M.D. Abramoff, M. Niemeijer, et al., *IEEE Trans. Med. Imaging* 23 (4) (2004) 501.
- [18] S.R. Aylward, E. Bullitt, *IEEE Trans. Med. Imaging* 21 (2) (2002) 61.
- [19] D. Marin, A. Aquino, M.E. Gegundez-Arias, et al., *IEEE Trans. Med. Imaging* 30 (1) (2011) 146.
- [20] M. Schaap, T.V. Walsum, L. Neeffes, et al., *IEEE Trans. Med. Imaging* 30 (11) (2011) 1974.
- [21] T.Y.P. Chui, D.A. VanNasdale, S.A. Burns, *Biomed. Opt. Express* 3 (10) (2012) 2537.
- [22] Y. Sato, J. Chen, R.A. Zoroofi, et al., *IEEE Trans. Biomed. Eng.* 44 (4) (1997) 225.
- [23] H. Bao, C. Rao, Y. Zhang, et al., *Opt. Lett.* 34 (22) (2009) 3484.
- [24] J. Tam, J.A. Martin, A. Roorda, *Invest. Ophthalmol. Vis. Sci.* 51 (3) (2010) 1691.
- [25] J. Rha, R.S. Jonnal, K.E. Thorn, et al., *Opt. Express* 14 (10) (2006) 4552.
- [26] M. Sofka, C.V. Stewart, *IEEE Trans. Med. Imaging* 25 (12) (2006) 1531.
- [27] J. Jan, J. Odstrcilik, *Comput. Med. Imaging Graph.* 36 (2012) 431.
- [28] C. Harris, M. Stephens, A Combined corner and edge detector, in: Proceedings on Fourth Alvey Vision Conference, Manchester, UK, 1988, pp. 147–151.